NASA TECHNICAL MEMORANDUM 100578

PLY-LEVEL FAILURE ANALYSIS OF A GRAPHITE/EPOXY LAMINATE UNDER BEARING-BYPASS LOADING

R. A. NAIK and J. H. CREWS, JR.

MARCH 1988

National Aeronautics and Space Administration

Langley Research Center
Hampton, Virginia 23665

SUMMARY

A combined experimental and analytical study has been conducted to investigate and predict the failure modes of a graphite/epoxy laminate subjected to combined bearing and bypass loading. Tests were conducted in a test machine that allowed the bearing-bypass load ratio to be controlled while a single-fastener coupon was loaded to failure in either tension or compression. Test coupons consisted of 16-ply, quasi-isotropic, T300/5208 graphite/epoxy laminates with a centrally-located 6.35-mm bolt having a clearance fit. Onset and ultimate failure modes and strengths were determined for each test case. The damage-onset modes were studied in detail by sectioning and micrographing the damaged specimens. A two-dimensional, finite element analysis was conducted to determine lamina strains around the bolt hole. Damage onset consisted of matrix cracks, delamination, and fiber failures. Stiffness loss appeared to be caused by fiber failures rather than by matrix cracking and delamination. Fiber failures in the 0 deg plies in the net-section tension and net-compression modes followed the matrix cracking direction in the adjacent 45 deg plies. Fiber failures associated with bearing damage were of two different types; compressively loaded fibers in the 0 deg plies failed by crushing whereas fibers in the 90 deg plies failed in tension. An unusual offset-compression mode was observed for compressive bearing-bypass loading in which the specimen failed across its width along a line offset from the hole. The computed lamina strains in the fiber direction were used in a combined analytical and experimental approach to predict bearing-bypass diagrams for damage onset from a few simple tests.

NOMENCLATURE

d	hole diameter, m
P_a	applied load, N
P_b	bearing load, N
P_p	bypass load, N
S_b	nominal bearing stress, MPa
S_{np}	nominal net-section bypass stress, MPa
r, θ	polar coordinates, m, deg
t	specimen thickness, m
w	specimen width, m
β	bearing-bypass ratio
ϵ_1	strain in fiber direction
ϵ_x^{tu}	longitudinal tensile ultimate strain for a 0 deg unnotched laminate
ϵ_y^{tu}	tranverse tensile ultimate strain for a 0 deg unnotched laminate
ϵ_x^{cu}	longitudinal compressive ultimate strain for a 0 deg unnotched laminate

INTRODUCTION

In the past, composite joints have often been designed using rather simple metals-based procedures. However, in contrast to metals, composites exhibit complex failure modes. Before analytical design procedures can be developed for composite joints, these failure modes must be better understood for loading conditions similar to those in multi-fastener joints.

Within a multi-fastener structural joint, fastener holes may be subjected to the combined effects of bearing loads and loads that bypass the hole, as illustrated in figure 1. The ratio of the bearing load to the bypass load depends on the joint stiffness and configuration. As the joint is loaded, this bearing-bypass ratio at each fastener remains nearly constant until damage begins to develop. In general, different bearing-bypass ratios can produce different failure modes and strengths for each fastener hole. The laminate response can be studied by testing single-fastener specimens under combined bearing-bypass loading, but such tests are usually difficult. A relatively simple test system that can simultaneously apply bearing and bypass loads was developed in reference 1. This test system used two hydraulic servo-control systems to apply proportional bearing and bypass loads to a laminate specimen with a central bolt hole. Damage-onset strengths and failure modes, for a graphite/epoxy laminate, were successfully measured, in reference 1, for a wide range of bearing-bypass load ratios in both tension and compression. The trends in the data were explained by using computed laminate stresses. Ultimate and damage-onset strengths and failure modes were reported, in reference 2, for a graphite/epoxy laminate tested using the same test apparatus. Laminate stresses were used along with appropriate failure criteria to predict the trends in the data, on a laminate level, for damage onset and ultimate failures.

The first objective of this study was to investigate, on a ply level, the damage-onset failure modes of a graphite/epoxy laminate subjected to simultaneous bearing and bypass loading over a range of bearing-bypass load ratios in both tension and compression. The test specimens were made of T300/5208 graphite/epoxy in a 16-ply quasi-isotropic layup. The bearing loads were applied through a clearance-fit steel bolt having a nominal diameter of

6.35 mm. The test results were plotted as bearing-bypass strength diagrams for damage onset and ultimate failure. The corresponding damage modes were determined by radiographing and sectioning the specimens after testing.

The second objective of this study was to analyze the bearing-bypass test results using the local lamina strains around the bolt hole, computed for combined bearing and bypass loading. These strains were calculated using a finite element procedure that accounted for nonlinear bolt-hole contact [3]. The ply strains were used to explain observed fiber failures for the basic damage-onset failure modes. Predictions for the damage-onset failure modes and strengths were made using lamina strains in the fiber direction.

BEARING-BYPASS TESTING

Test Procedure

The test specimen configuration and loading combinations are shown in figure 2. The T300/5208 graphite/epoxy specimens were machined from a single $[0/45/90/-45]_{2s}$ panel. The bolt holes were machined using an ultrasonic diamond core drill and then carefully hand-reamed to produce a clearance of 0.076 mm with the steel bolts. This clearance, 1.2 percent of the hole diameter, is typical of aircraft joints.

The test system [1-3], shown in figure 3, consisted of two hydraulic servo-control systems that were used to independently load the two ends of the test specimen. The center of the specimen was bolted between two bearing-reaction plates which were attached to the load frame using two load cells. Any difference between the two end loads produced a bearing load at the

central bolt hole. This bearing load was measured by the load cells under the bearing-reaction plates. The end loads were syncronized by a common input signal; as a result, a constant bearing-bypass ratio was maintained throughout each test. During compression, the bearing-reaction plates prevented specimen buckling. Hardened steel bushings were used between the bolt and the bearing-reaction plates. These 12.7-mm bushings were machined for a sliding fit, allowing the bolt clamp-up force to be transmitted to the local region around the bolt hole. This arrangement was equivalent to having a clamp-up washer directly against the side of the specimen, as was used in references 1-5. The bolt was tightened by a 0.2 Nm torque to produce a very small clamp-up force (finger tight) against the specimen.

The loading notations for tension and compression testing are shown in figure 2(b). All tests were conducted at a slow loading rate of 3.75 N/s. The results are reported in terms of nominal bearing stress S_b and nominal net-section bypass stress S_{np}, calculated using the following equations:

$$S_b = P_b / td$$

$$S_{np} = P_p / t\,(w - d)$$

where t is specimen thickness and w is the width. The bearing-bypass ratio β is defined as

$$\beta = S_b / S_{np}$$

Throughout each test, displacement transducers on each side of the specimen were used to measure the relative displacement between the stationary

bolt and the end of the specimen test section over a gage length of 46.4 mm (figure 2(a)). These displacement measurements were used to determine the onset of damage. The bearing and bypass loads were plotted against the specimen displacement. The bypass load variation with specimen displacement is shown for a typical case in figure 4. Both the bearing and bypass curves had a small initial nonlinearity, caused by varying bolt-hole contact [6], but gradually developed a nearly linear response. At higher load levels, the curves gradually developed a second nonlinearity, which indicated damage at the bolt hole, as mentioned in reference 1. Because the change in linearity was so gradual, an offset of 0.001 of the hole diameter, d, was selected to define the damage-onset load, as indicated in figure 4. Some specimens were unloaded after the damage-onset load level, treated with an X-ray opaque dye-penetrant, and radiographed to determine the damage-onset mode. Other specimens were sectioned and micrographed to analyze ply damage.

Test Results

Figure 5 shows radiographs of four damage-onset modes. For tension dominated loading, the damage developed in the net-section tension (NT) mode, figure 5(a). The gray shadows show delaminations and the dark bands indicate ply cracks. The tension-reacted bearing (TRB) and the compression-reacted bearing (CRB) damage modes are quite similar, as expected. The net-section compression (NC) mode involves rather discrete damage zones extending from the hole. The three basic damage-onset modes, NT, bearing, and NC will be discussed in greater detail later.

The measured S_b and S_{np} values corresponding to damage onset and ultimate failure are given in Table 1 and are also plotted in figure 6, on a

bearing-bypass diagram [2,3]. The open and filled symbols represent damage onset and ultimate failure, respectively. Each symbol represents the average of three tests and the tick marks indicate the range of the measured strengths, plotted along lines of constant β.

The bearing-bypass diagram (figure 6) for damage onset (open symbols) shows some expected and also unexpected results. The right side of the bearing-bypass diagram for damage onset (open symbols) shows tension results for four β values (0, 1, 3, ∞). The open symbol on the positive S_{np} axis represents the all-bypass loading case in tension ($\beta = 0$). The NT next to the symbol indicates net-section tension damage. As discussed in reference 7, all of the test cases with NT damage can be represented by a straight line and, thus, show a linear interaction. This linearity suggests that the local stresses due to bearing loading and those due to bypass loading each contribute directly to failure. The horizontal "bearing-cutoff" lines were drawn through the $\beta = \infty$ data points for onset and ultimate strengths. The damage-onset strengths for the all-bearing tension case ($\beta = \infty$) and the all-bearing compression case ($\beta = -\infty$) differ by about three percent. The bearing-cutoff line used for tension damage onset does not appear to apply for compression damage onset, because for $\beta = -1$, the CRB damage was found at a much lower strength level. The compressive bypass load had a somewhat unexpected effect on the onset of bearing damage. The lower bearing onset strength for combined bearing and bypass loading was analyzed in reference 1 and was shown to result from a decrease in the bolt-hole contact angle caused by the compressive bypass load. For the all-bypass compressive loading ($\beta = -0$), the open symbol on the negative S_{np} axis represents the open hole case. The NC damage, for this case, initiated at -332 MPa. The solid symbol on the negative S_{np} axis represents both damage onset and ultimate

catastrophic failure for the filled hole (with bolt) case. The NC damage for the filled-hole case initiated at -422 MPa, which is 27 percent larger than the open hole case. The filled hole case involved "dual" bolt-hole contact in which the applied bypass load caused the hole to collapse on the bolt and make contact along two diametrically opposite arcs. This dual-contact allowed load transfer across the hole and, therefore, produced a higher strength than for the open-hole case [2].

Figure 6 provides a comparison of onset and ultimate strengths for the full range of tension and compression bearing-bypass loading. For all-bypass loading (β = 0 and -0), the specimens failed soon after damage onset. In contrast, for the all bearing loading (β = ∞ and -∞), the specimens failed at considerably higher loads than required to initiate damage. The clampup bushings constrained the brooming produced during bearing failures and thereby strengthened the laminate as the bearing damage developed. When bearing and bypass loads were combined, the specimens also showed additional strength after damage onset, especially in compression. A comparison of the damage modes in figure 6 shows that the onset-damage mode was the same as the ultimate failure mode in most cases. The exception occurred for the compressive bearing-bypass loading. For β = -3, the damage initiated in the CRB mode, and for β = -1, damage initiated in the CRB/NC mode, but the specimen failed in a different mode, referred to here as the offset-compression (OSC) mode, in which the specimen failed along a line parallel to the net-section and offset from the hole center (see figure 7). The amount of offset was equal to the radius of the clampup bushings around the bolt hole [3]. This failure was typical of a compression failure but developed away from the specimen net-section. This transition from the CRB damage-onset mode to the OSC failure mode could also happen in muti-fastener joints and,

therefore, may be an additional complication when joint strength predictions are made for compressive loadings.

STRESS ANALYSIS

When a bolt clearance is used, as in the present study, the contact angle at the bolt-hole interface varies nonlinearly with applied load [6,10]. Using the inverse technique described in reference 6, this nonlinear problem is reduced to a linear problem. In this technique, for a simple bearing loading, a contact angle is assumed and the corresponding bearing load is calculated. This procedure is then repeated for a range of contact angles to establish a relationship between contact angle and bearing load. In reference 10, this technique was extended to include combined bearing and bypass loading. For each bearing-bypass ratio β, the combined bearing and bypass loading was expressed in terms of bearing stress S_b and β. Thus, for a given β, the procedure was identical to that used in reference 6. This procedure was repeated to establish a relationship between contact angle and bearing-bypass loading for each β value in the test program.

These calculations were done using the NASTRAN finite element code. This code is well suited for the inverse technique because the contact of the bolt and the hole can be represented using displacement constraints along a portion of the hole boundary [3,6]. Displaced nodes on the hole boundary were constrained to lie on a circular arc corresponding to the bolt surface. This represented a rigid bolt having a frictionless interface with the hole. A very fine two-dimensional mesh [3,6] was used to model the test specimen.

Along the hole boundary, elements subtended less than 1^0 of arc. As a result, the contact arc could be modelled very accurately.

ANALYSIS OF DAMAGE-ONSET MODES

The NT, bearing, and NC damage-onset modes are discussed using lamina strains and micrographs of sections around the damaged holes. As mentioned earlier, damage onset at the bolt hole was detected by an offset of the load-displacement curve (figure 4) recorded during each test. However, damage at the bolt hole could be in the form of matrix cracking, delamination, fiber failure, or a combination of all three. In the next section, computed ply strains are used to discuss micrographs of laminates loaded up to the measured damage-onset strengths.

Net-Tension Damage

Figures 8 and 9 show the lamina strains ϵ_2 and ϵ_1, respectively, calculated around the hole boundary for the all-bypass tension loading case ($\beta = 0$) using the measured strength of $S_{np} = 304$ MPa. The peak ϵ_2 strains, in figure 8, in the 90 deg and ± 45 deg plies greatly exceed the transverse tensile ultimate strain, ϵ_y^{tu}, of 0.0036 [8] for a 0-deg unidirectional laminate. Note that the value of ϵ_y^{tu} is a structural property that varies with constraint and ply thickness. The high ϵ_2 strains, in figure 8, probably caused the matrix cracking seen in the micrograph in figure 10(a). This widespread matrix cracking and delamination must have developed without causing any detectable change in specimen stiffness. This suggests that fiber

failures were probably the main cause of the measured stiffness change at damage onset. Emphasis will, therefore, be placed on fiber strains in the remainder of this paper.

In figure 9, the 0 deg ply has a peak ϵ_1 strain of about 0.0137 near $\theta = 90^0$. This computed peak value exceeds the unnotched tensile ultimate strain, ϵ_x^{tu}, of 0.011 [8] for a 0 deg unidirectional laminate. Part of this discrepancy can be explained by the fact that the peak local strain acts over a very small volume of material [11] subjected to a high stress gradient. The peak local strength should be higher than the unnotched strength obtained using a relatively large tensile coupon under uniform stress. Also the matrix cracking and delamination (see figure 10(a)) reduced the NT strain concentration for the region of peak ϵ_1 strain. Because the stress analysis did not account for this reduction, the computed peak ϵ_1 was somewhat overpredicted. However, this computed peak strain of 0.0137 should agree with similar peak values for other cases of NT damage onset. The peak value of $\epsilon_1 = 0.0137$, will, therefore be used in subsequent analyses to predict critical conditions for the onset of NT damage.

Figure 10(a) shows a micrograph of NT damage at section A-A for a specimen loaded until damage onset was detected by a change in the slope of the load-displacement curve. The matrix cracking that was visible in figure 5(a) in the $\pm$45 deg plies is also visible in the micrograph. Cracking is also visible in the 90 deg plies. In most cases delaminations along interfaces with adjacent plies seem to be associated with matrix cracking.

Fiber failure, in figure 10(a), is evident in the 0 deg plies near $\theta = 90^0$, as would be expected from the peak ϵ_1 in figure 9. The location of the fiber failure appears to be associated with the matrix cracking in the adjacent 45 deg plies (see inset). Figure 10(b) shows a plan view of the

fiber failure in the 0 deg ply. The fiber failure seems to follow the direction of matrix cracking in the adjacent 45 deg ply. A similar observation was made by Jamison [9] where fiber failures in the 0 deg plies were found to correspond to the location of matrix cracks in the neighboring 90 deg plies of a $[0/90_2]_s$ laminate of T300/5208 loaded in uniaxial tension.

Bearing Damage

Figure 11 shows the lamina strains in the fiber direction, ϵ_1, for the tension bearing case ($\beta = \infty$) calculated around the hole boundary using the measured strength of $S_b = 542$ MPa. The 0-deg ply has a compressive peak strain of about -0.013 near $\theta = 0^o$. The discrepancy between this peak value and the ϵ_x^{cu} of -0.0086 for an unnotched unidirectional laminate are believed to be explained by the same volume dependence on failure [11] arguments discussed earlier for the NT case. The sudden change in the slope of the curves near 60^o is caused by the contact at the bolt-hole interface. Contact between the bolt and the hole, for this bearing loaded case, extends from 0^o to 59^o at a bearing load level of 542 MPa. The compression bearing case, $\beta = -\infty$, had a peak ϵ_1 of -0.0136 in the 0 deg ply near $\theta = 0^o$, calculated for a measured strength of $S_b = 528$ MPa. The peak strains of -0.013 and -0.0136, calculated for the simple bearing cases in tension and compression, respectively, will be used as critical strains to predict the onset of TRB and CRB damage.

Figure 12(a) shows a micrograph of bearing damage for section B-B for a specimen loaded up to damage onset. Damage appears to be concentrated near the outer surface plies. Matrix cracking is evident in the 0 deg and 45 deg plies. Delaminations are visible along the 0/45 and 45/90 interfaces. Fiber

failures in the 90 deg plies are also visible (see inset) and seem to be associated with transverse cracking in the 90 deg plies. The fiber failures in the 90 deg plies are probably caused by the high tensile strains near $\theta = 0^0$ shown in figure 11. However, the critical fiber failures appear to be located in the 0 deg plies in the same region, near $\theta = 0^0$, as shown in figure 12(b). The crushing failures of these fibers in the 0 deg ply also correlate well with the peak ϵ_1, near $\theta = 0^0$, shown in figure 11.

Net-Section Compression Damage

Hole-boundary lamina strains, ϵ_1, for compression bypass loading are shown in figure 13. These results correspond to a bypass stress S_{np} of -422 MPa. The 0 deg ply has a compressive peak strain of about -0.0163 near $\theta = 90^0$. The discrepancy between this peak value and the ϵ_x^{cu} of -0.0086 for an unnotched unidirectional laminate can be explained by similar volumetric arguments made for the NT case discussed earlier. The sudden changes in the slope of the curves at around 20^0 and 160^0 are caused by the change in the contact conditions between the bolt and the hole at those points. For this case of compression bypass loading, dual contact extends around the hole from 0^0 to 20^0 and from 160^0 to 180^0 at a bypass load level of -422 MPa. The computed peak strain, $\epsilon_1 = -0.0163$, corresponding to NC damage for the $\beta = -0$ case, which involves dual contact, should agree with similar peak values for other cases with NC damage. As shown in figure 6, the open hole case with compressive loading also showed NC damage with an onset strength of $S_{np} = -332$ MPa. At this load level, the computed peak ϵ_1 is -0.0164, which agrees well with the computed peak of -0.0163 for the NC case with dual contact. The computed peak value of $\epsilon_1 = -0.0164$ for the simple

open hole compression case will be used later to predict the onset of NC damage.

A micrograph of NC damage is shown in figure 14(a), across a section D-D, for a specimen loaded up to damage onset. There appears to be less delamination, in this case, compared to the bearing case discussed earlier. Matrix cracking is evident in the 45 deg plies along with associated delaminations between the 45/90 interfaces. The compressive fiber failures in the 0 deg plies also seem to be associated with the matrix cracks in the adjacent 45 deg plies. The peak ϵ_1 strain in figure 13 correlates well with the observed fiber failures at $\theta = 90^{o}$. A closer view (see inset) of the fiber failure indicates evidence of microbuckling. A plan view of a polished 0 deg ply, in figure 14(b), indicates fiber failures along ± 45 deg which seem to correspond to the matrix cracks in the neighboring 45 deg plies.

The results in this section demonstrate that local lamina strains in the fiber direction correlate well with the observed fiber failures in the three basic failure modes of NT, bearing, and NC.

DAMAGE-ONSET PREDICTIONS

Based on the discussion in the previous section, damage initiation, as detected by a change in stiffness of the specimen, appears to be governed by the peak ply strain in the fiber direction. The onset of damage will be assumed to occur when the peak ϵ_1 in a ply reaches a critical value for each damage mode. The following critical ϵ_1 values were calculated, for each damage mode, using simple tension, compression, and bearing data in the previous section: 0.0137 for NT, -0.013 for TRB, -0.0136 for CRB, and -0.0164

for NC. Figure 15 shows the damage onset predictions for various bearing-bypass loads. The solid lines represent the damage-onset strengths calculated using the critical ϵ_1 values above. The average damage-onset strength data from figure 6 are replotted as open symbols in figure 15. For $\beta = -1$, an unconservative prediction is made due the presence of NC damage which is not accounted for in the analysis. For β values between about -0.5 to -0, there is dual contact [1-3] between the bolt and the hole. Further testing will be required to verify the predictions in this region. The calculated curves agree reasonably well with the data trends for strength. Also, the calculated damage modes agree with those discussed earlier. This demonstrates that damage-onset modes and strengths can be predicted from the peak hole-boundary lamina strains if critical strain values for each damage mode are known.

The correlation between the strength calculations and the strength measurements in figure 15 suggests that a combined analytical and experimental approach could be used to predict bearing-bypass diagrams for damage onset from a few simple tests. Such tests could be conducted for the all-bypass ($\beta = 0$), all-bearing ($\beta = \infty$ and $\beta = -\infty$) and open hole compression cases to determine the critical ply strains, which could then be used with a stress analysis to construct curves for the more complicated cases of bearing-bypass loading.

CONCLUDING REMARKS

A combined experimental and analytical study has been conducted to investigate the failure modes of a graphite/epoxy (T300/5208) laminate subjected to combined bearing and bypass loading. Tests were conducted on

single-fastener specimens loaded in either tension or compression. Test specimens consisted of 16-ply, quasi-isotropic graphite/epoxy laminates with a centrally located hole. Bearing loads were applied through a steel bolt having a clearance fit. Damage-onset, ultimate strengths, and the corresponding failure modes were determined for each test case. Specimens were sectioned and micrographed to study damage-onset modes in detail. A finite element procedure was then used to calculate the local lamina strains around the bolt hole. Predictions for damage onset were made based on these calculated strains.

Damage onset detected by a change in the stiffness of the specimen, was found to be governed by fiber failures rather than by matrix cracks and delamination. Fiber failures in the 0 deg plies, in the net-section tension failure mode, followed the matrix cracking direction in the adjacent 45 deg plies. Fiber failures associated with bearing damage onset were of two different types; compressively loaded fibers in the 0 deg plies failed by crushing whereas fibers in the 90 deg plies failed in tension. In the net-section compression mode, fiber failures occurred in the 0 deg plies by microbuckling and followed the matrix cracking direction in the adjacent 45 deg plies.

Failure modes associated with ultimate strength were usually the same as the corresponding onset mode. The exception occurred for the compressive bearing-bypass cases in which damage onset in the CRB mode led to an unusual offset-compression mode in which the specimen failed across its width along a line offset from the hole. In general, specimens failed immediately after damage onset when an all-bypass loading was used in both tension and compression. In contrast, for all-bearing loading, specimens failed at considerably higher loads than required to initiate damage. Also, when

bearing and bypass loads were combined, specimens failed at loads higher than that for damage onset. This was more noticeable in compression than in tension.

Local inplane lamina strains around the hole, obtained by a two-dimensional finite-element analysis that accounted for bolt-hole clearance correlated well with the observed fiber failures. Damage-onset strengths and failure modes were predicted using hole-boundary lamina strains in the fiber direction, using a critical strain for each damage mode. A combined analytical and experimental approach can probably be used to predict bearing-bypass diagrams for damage onset from a few simple tests in tension, compression, and bearing.

REFERENCES

1. Crews, J. H., Jr. and Naik, R. A.: "Combined Bearing and Bypass Loading on a Graphite/Epoxy Laminate," Composite Structures, Vol. 6, 1986, pp. 21-40.
2. Crews, J. H., Jr. and Naik, R. A.: "Bearing-Bypass Loading on Bolted Composite Joints," NASA TM 89153, National Aeronautics and Space Administration, May 1987. Also presented at the AGARD Specialists' Meeting on Behavior & Analysis of Mechanically Fastened Joints in Composite Structures, April 27-29, 1987, Madrid, Spain.
3. Naik, R. A.: "An Analytical and Experimental Study of Clearance and Bearing-Bypass Load Effects in Composite Bolted Joints," Ph.D. dissertation, Old Dominion University, Norfolk, Virginia, August 1986.
4. Crews, J. H., Jr.: "Bolt-Bearing Fatigue of a Graphite/Epoxy Laminate," Joining of Composite Materials, ASTM STP 749, K. T. Kedward, Ed., American Society for Testing and Materials, 1981, pp. 131-144.
5. Crews, J. H., Jr. and Naik, R. A.: "Failure Analysis of a Graphite/Epoxy Laminate Subjected to Bolt-Bearing Loads," Composite Materials: Fatigue and Fracture, ASTM STP 907, H. T. Hahn, Ed., American Society for Testing and Materials, 1986, pp. 115-133.
6. Naik, R. A. and Crews, J. H., Jr.: "Stress Analysis Method for a Clearance-Fit Bolt under Bearing Loads," AIAA Journal, Vol. 24, No. 8, August 1986, pp. 1348-1353.

7. Hart-Smith, L. J.: "Bolted Joints in Graphite/Epoxy Composites, NASA CR-144899, National Aeronautics and Space Administration, January 1977.

8. DOD/NASA Advanced Composites Design Guide, Vol. IV-A: Materials, First Edition, Contract No. F33615-78-C-3203, Air Force Wright Aeronautical Laboratories, July 1983. (Available as NASA CR-173407 and from DTIC as AD B080 184L.)

9. Jamison, R. D.: "The Role of Microdamage in Tensile Failure of Graphite/Epoxy Laminates," Composites Science and Technology, Vol. 24, 1985, pp. 83-99.

10. Naik, R. A. and Crews, J. H., Jr.: "Stress Analysis Method for Clearance-Fit Joints with Bearing-Bypass Loads," NASA TM-100551, National Aeronautics and Space Administration, 1988. (To be published.)

11. Phoenix, S. L.: "Statistical Aspects of Failure of Fibrous Materials," Composite Materials: Testing and Design (Fifth Conference), ASTM STP 674, S. W. Tsai, Ed., American Society for Testing and Materials, 1979, pp.455-483.

Table 1.- Laminate strengths under bearing-bypass loading for a T300/5208, $[0/45/90/-45]_{2s}$, graphite/epoxy laminate.

Bearing-bypass ratio, β	Damage-Onset			Ultimate Failure		
	S_b(MPa)	S_{np}(MPa)	Mode	S_b(MPa)	S_{np}(MPa)	Mode
Tension						
0	0	304	NT	0	330	NT
1	237	237	NT	263	263	NT
3	468	156	NT	648	216	NT
∞	542	0	TRB	812	0	TRB
Compression						
-0	0	-422	NC	0	-422	NC
-1	314	-314	CRB/NC	461	-461	OSC
-3	498	-166	CRB	759	-253	OSC
-∞	528	0	CRB	853	0	CRB

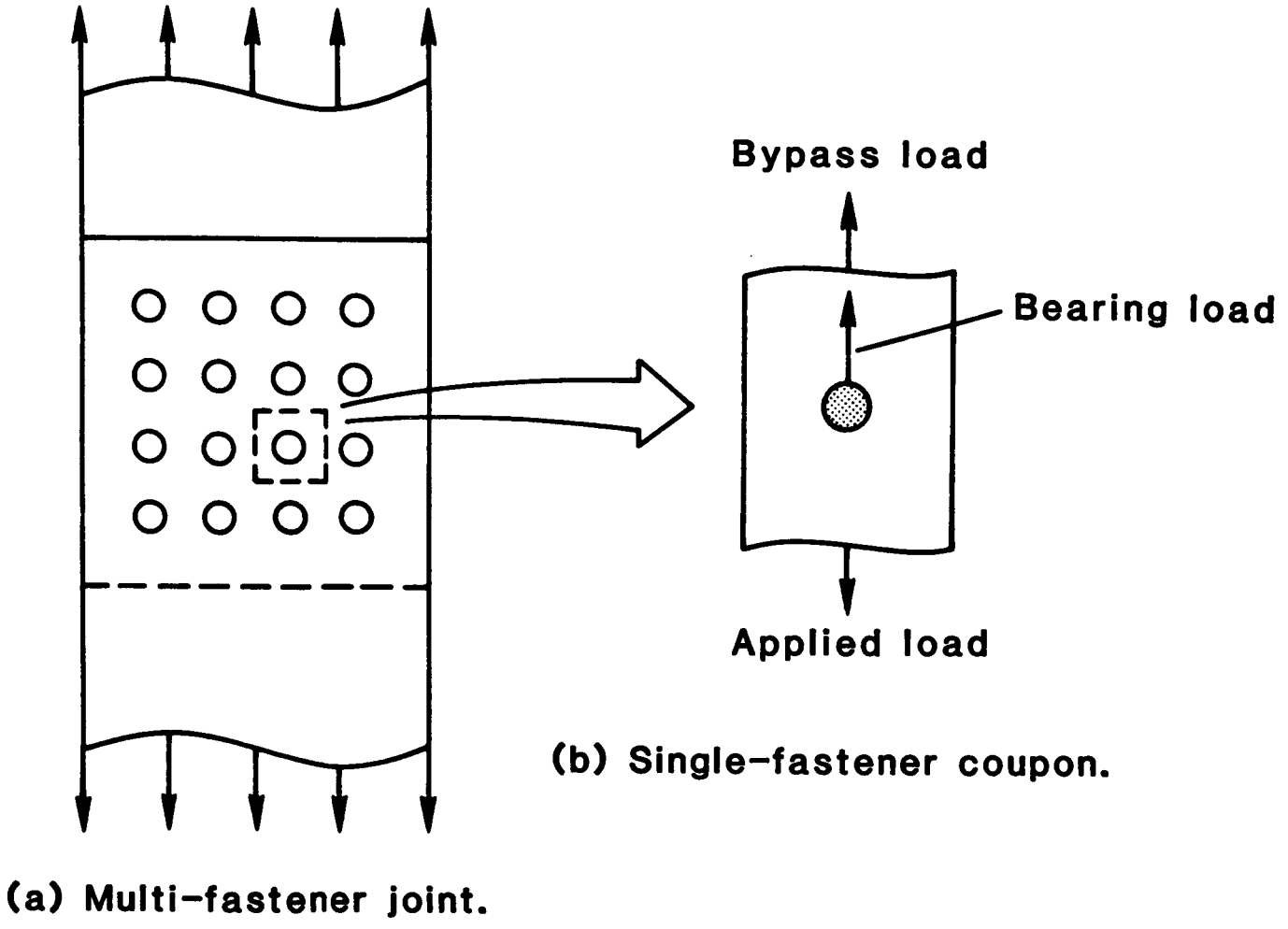

Figure 1.- Bearing-bypass loading within a multi-fastener joint.

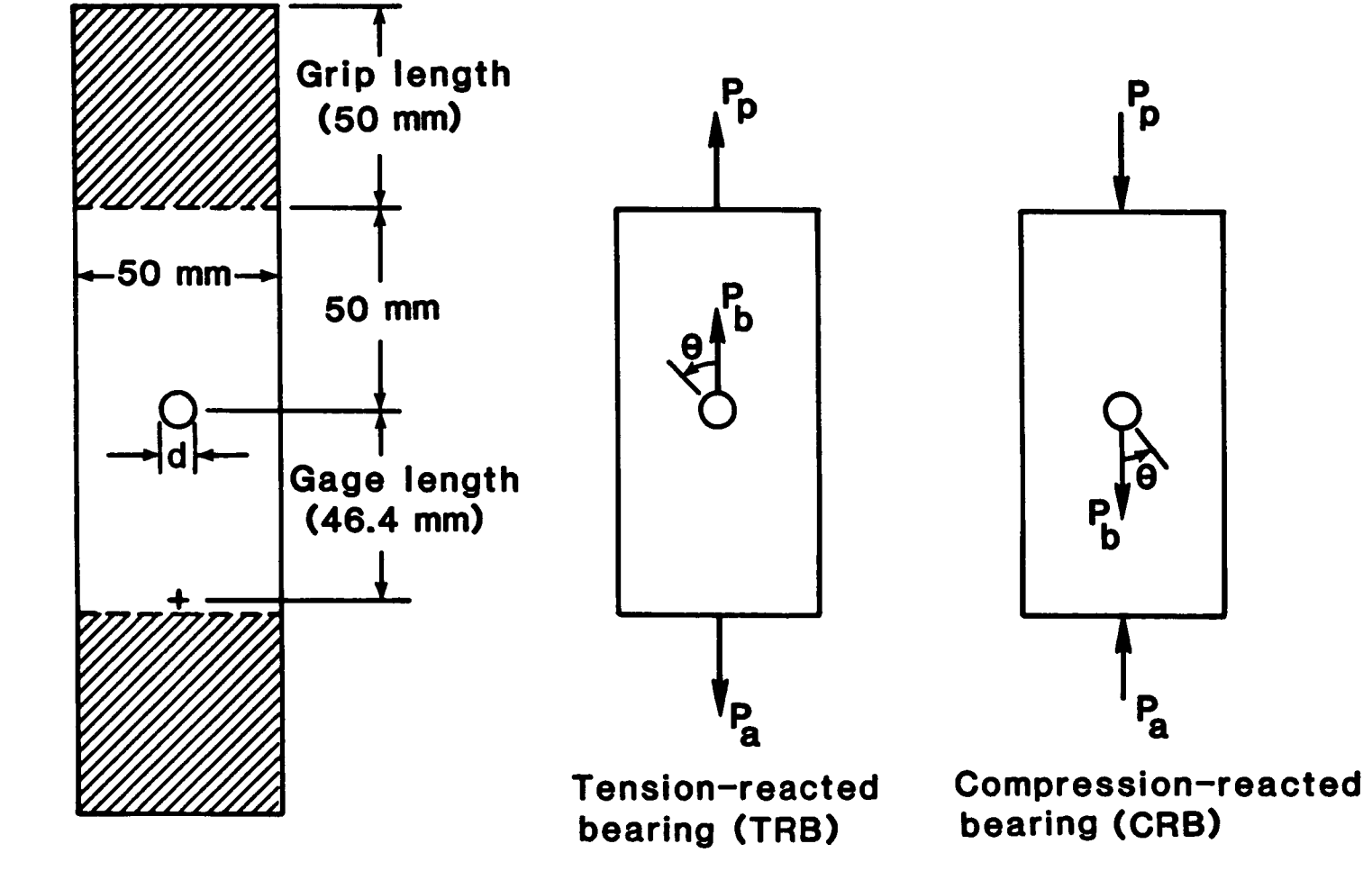

Figure 2.- Specimen configuration for bearing-bypass loading.

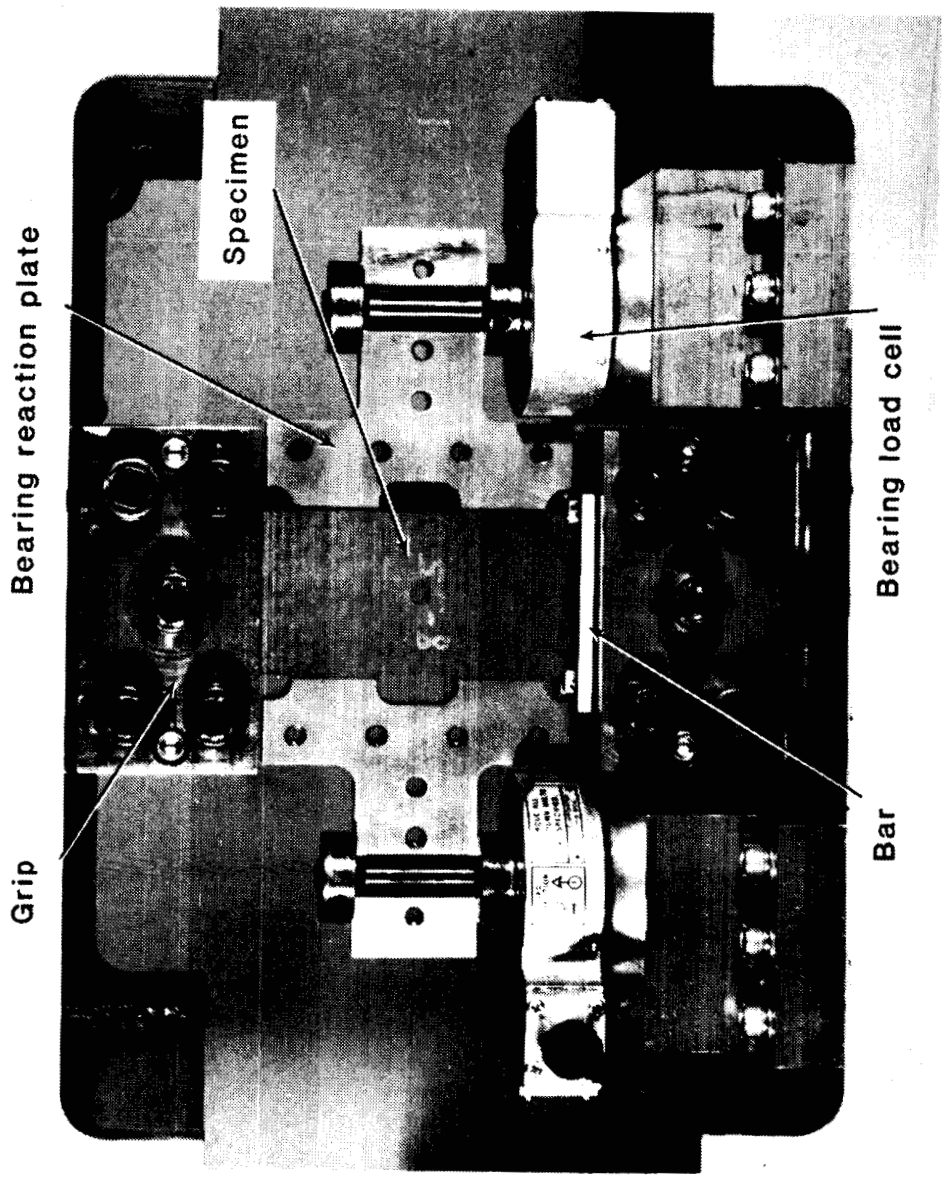

Figure 3.- Bearing-bypass test apparatus with front bearing-reaction plate removed.

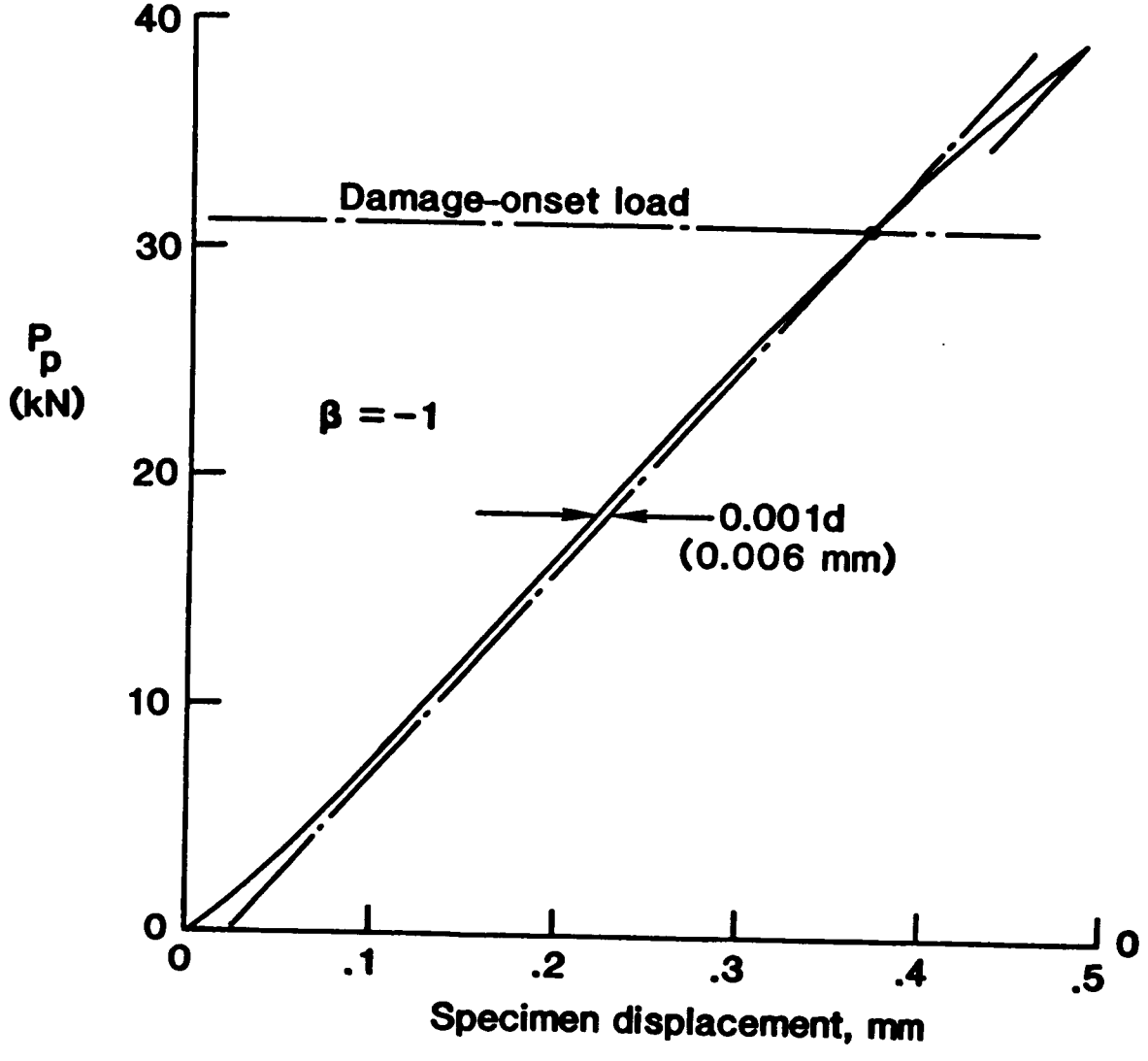

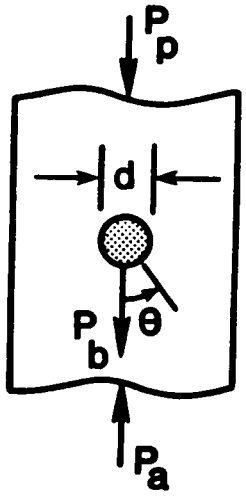

Figure 4.- Typical load-displacement curve.

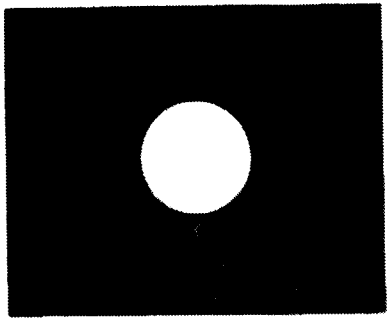

(a) Net-section tension (NT)

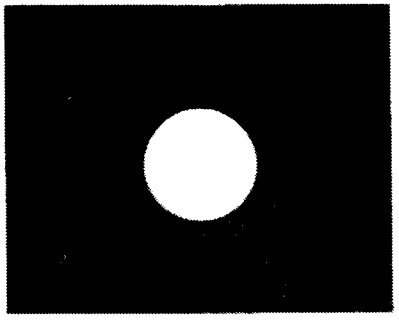

(b) Tension-reacted bearing (TRB)

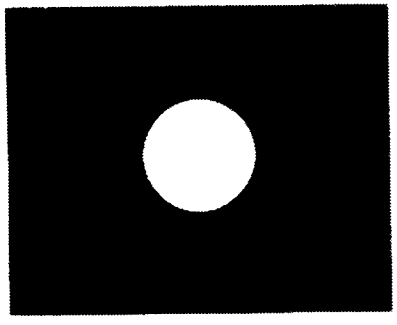

(c) Compression-reacted bearing (CRB)

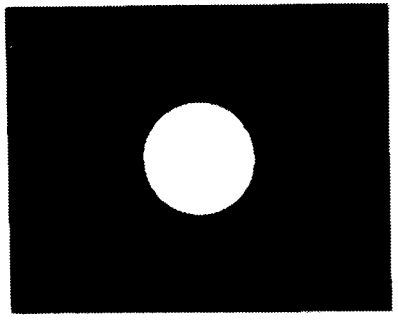

(d) Net-section compression (NC)

Figure 5.- Radiographs of damage-onset at fastener hole.

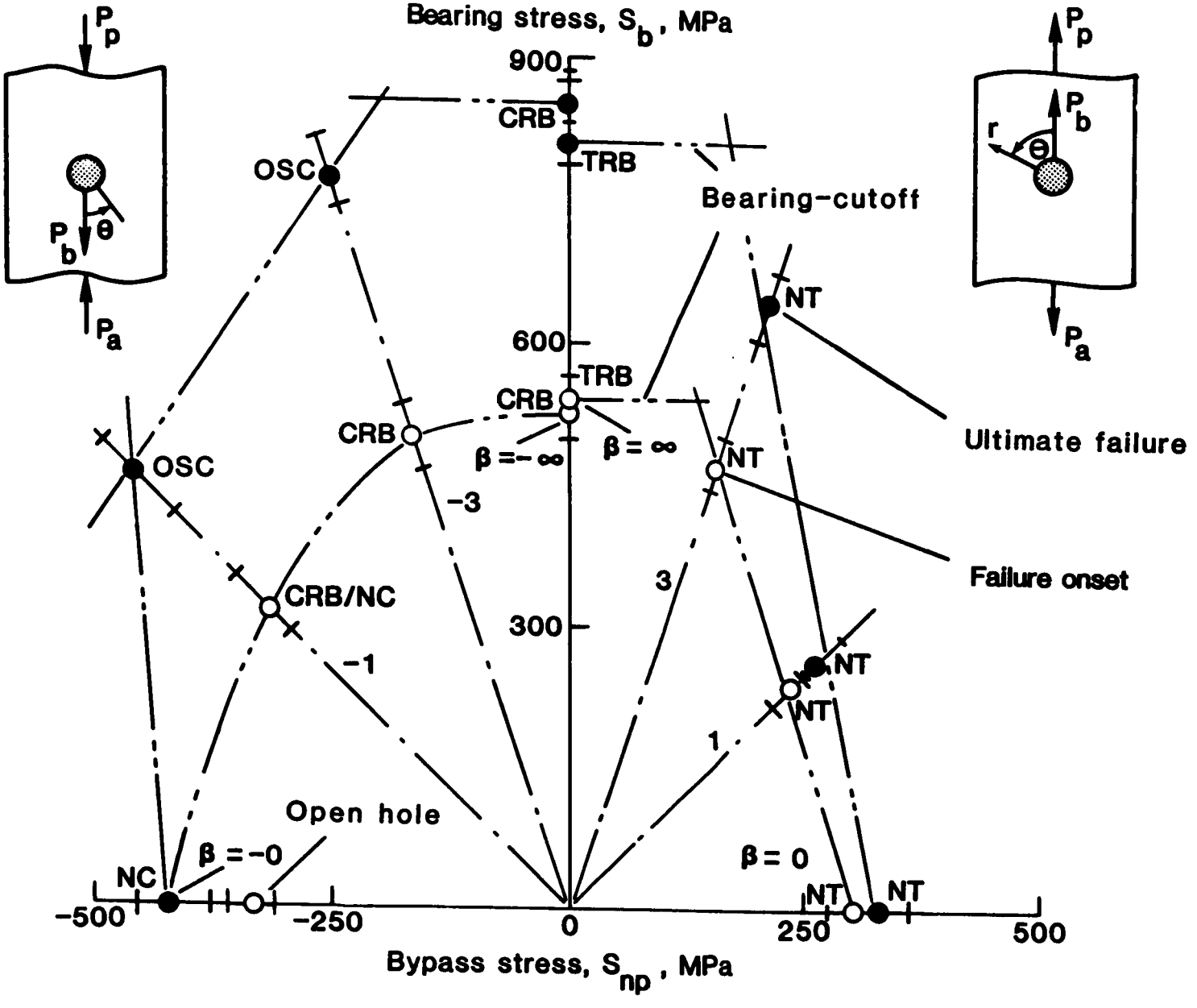

Figure 6.- Bearing-bypass diagram for ultimate and damage-onset strengths.

Figure 7.- Photograph of failed specimen showing OSC failure.

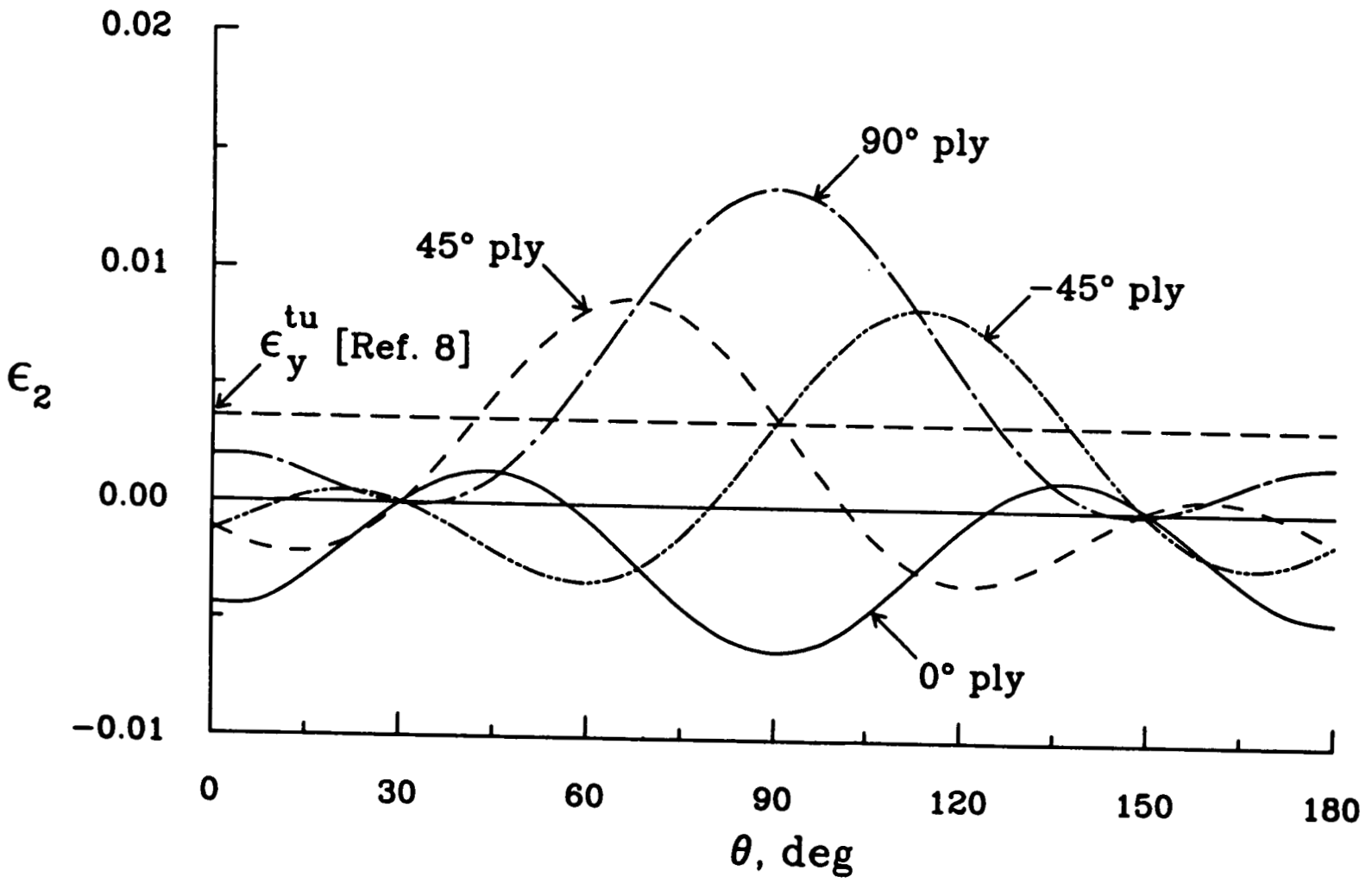

Figure 8.- Lamina ϵ_2 strains around hole boundary for NT damage onset (S_{np} = 304 MPa)

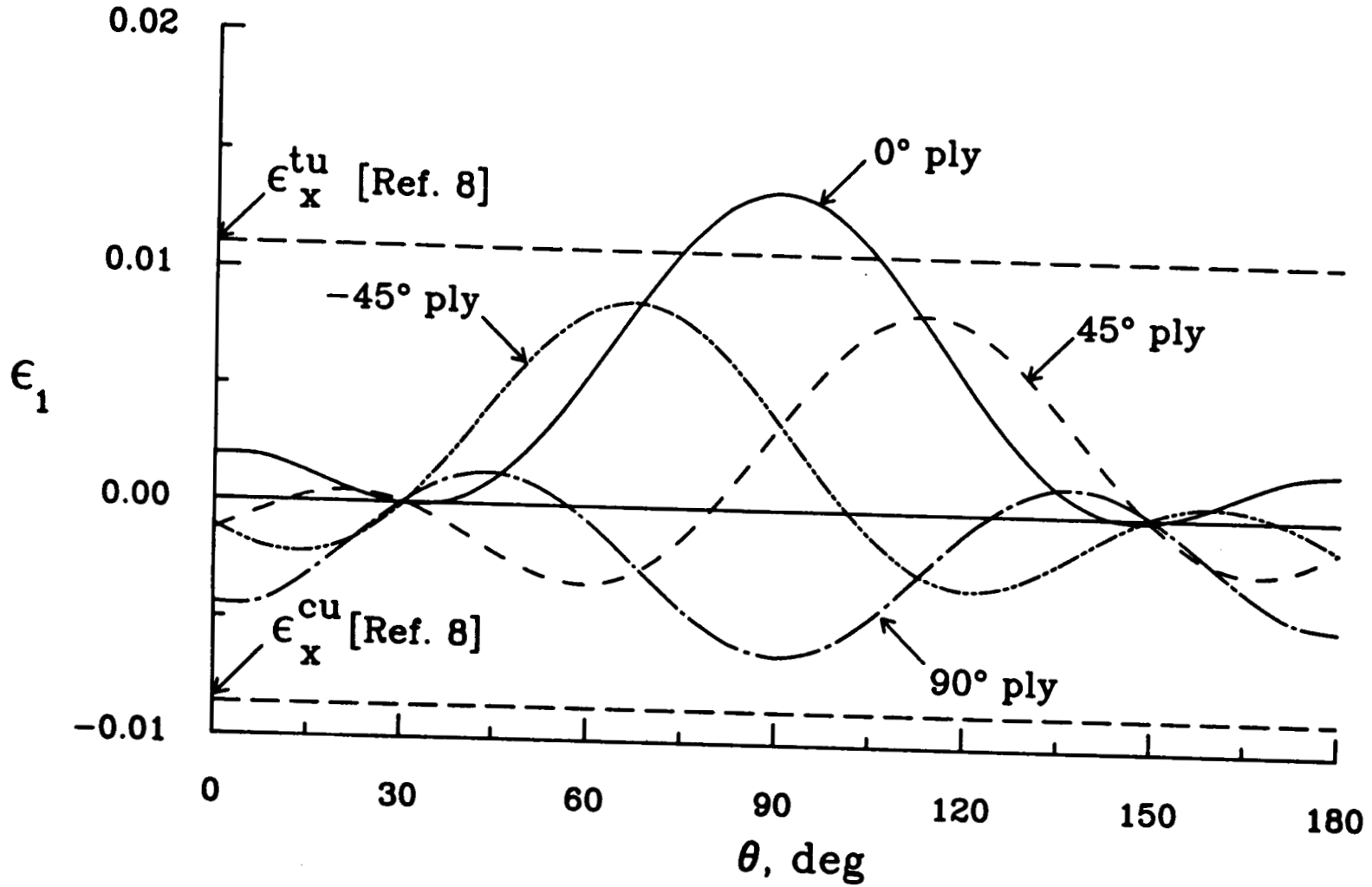

Figure 9.- Lamina ϵ_1 strains around hole boundary for NT damage onset (S_{np} = 304 MPa).

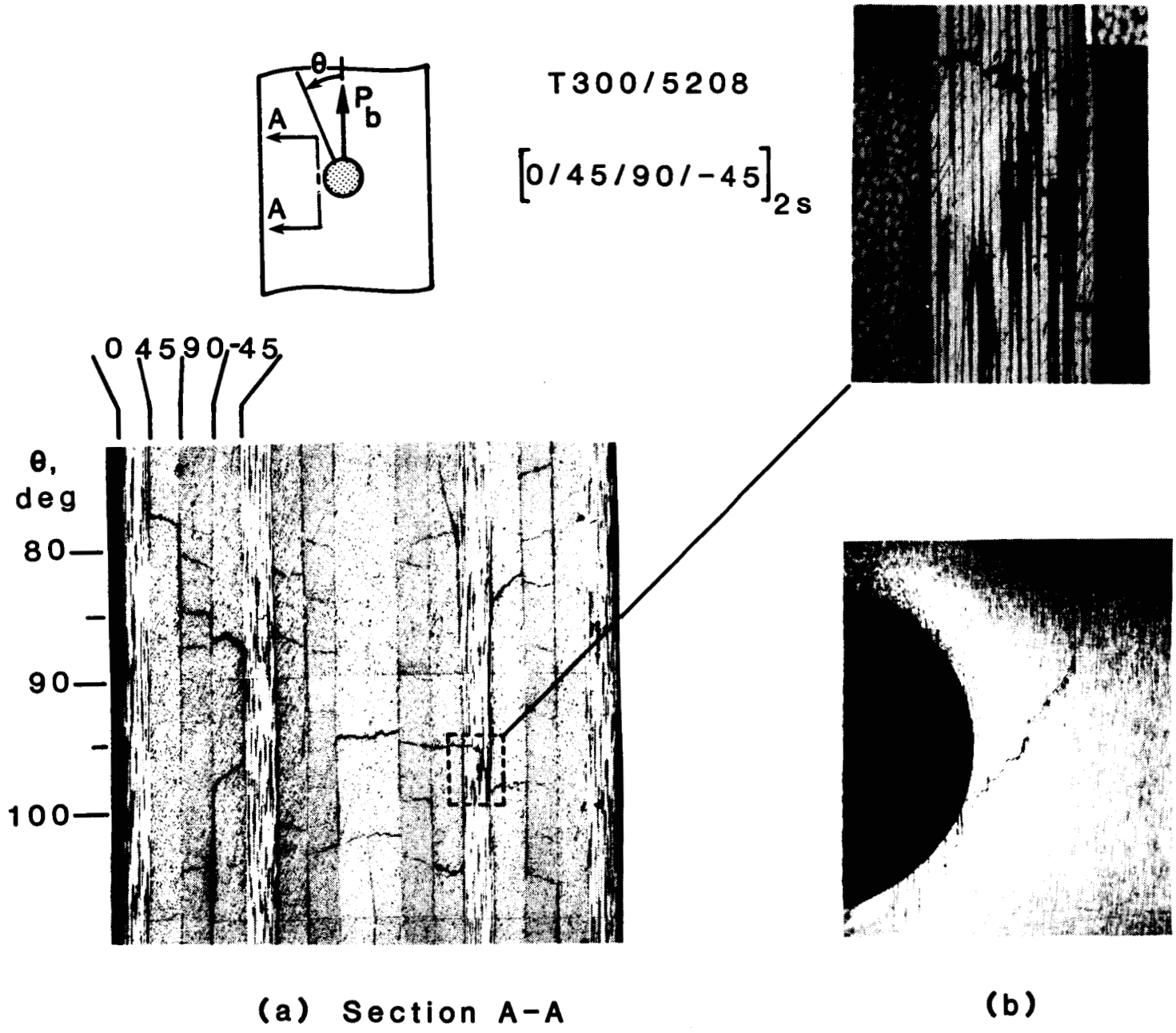

Figure 10.- Micrographs of NT damage onset.

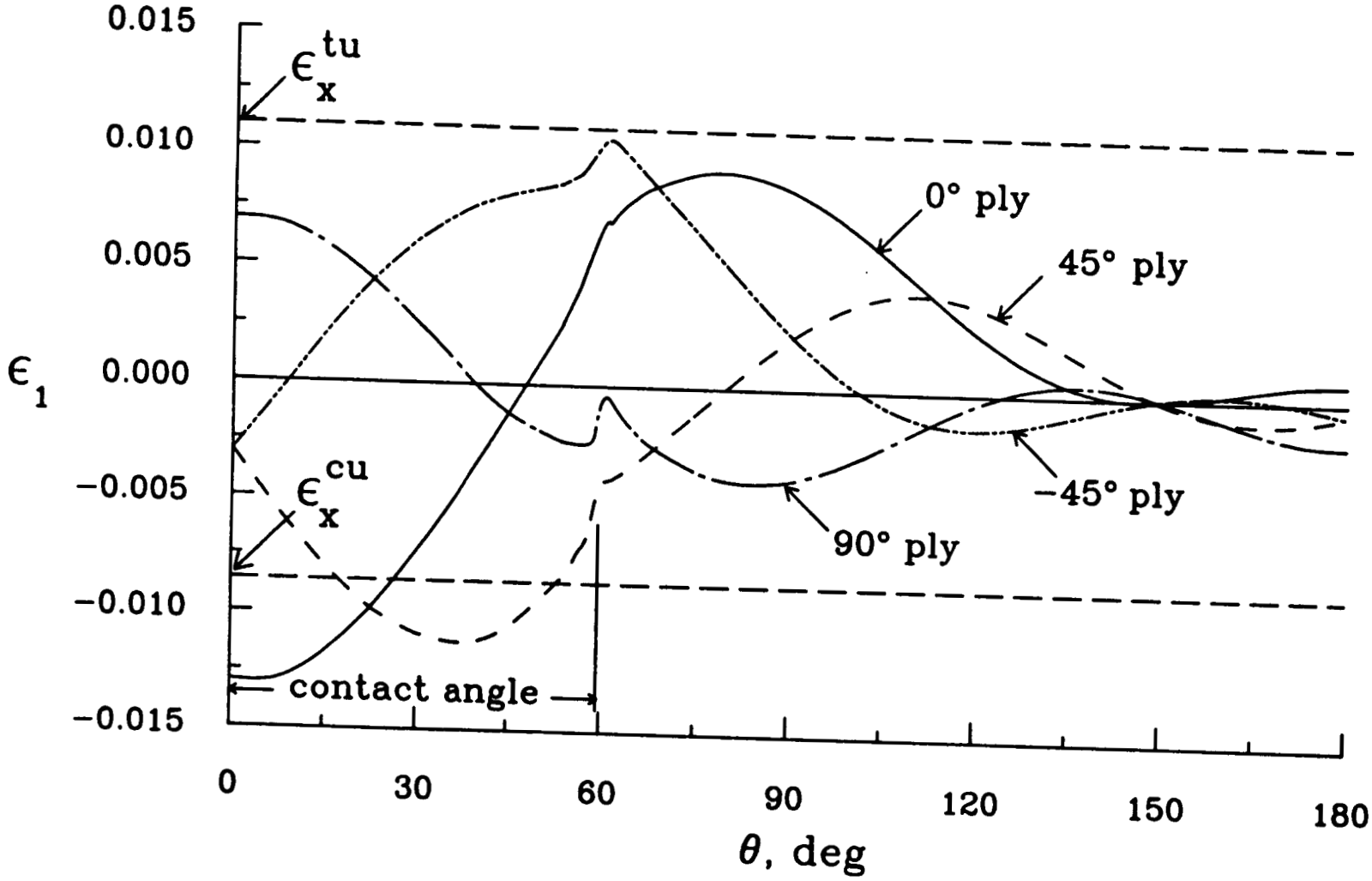

Figure 11.- Lamina ϵ_1 strains around hole boundary for TRB damage onset (S_b = 542 MPa).

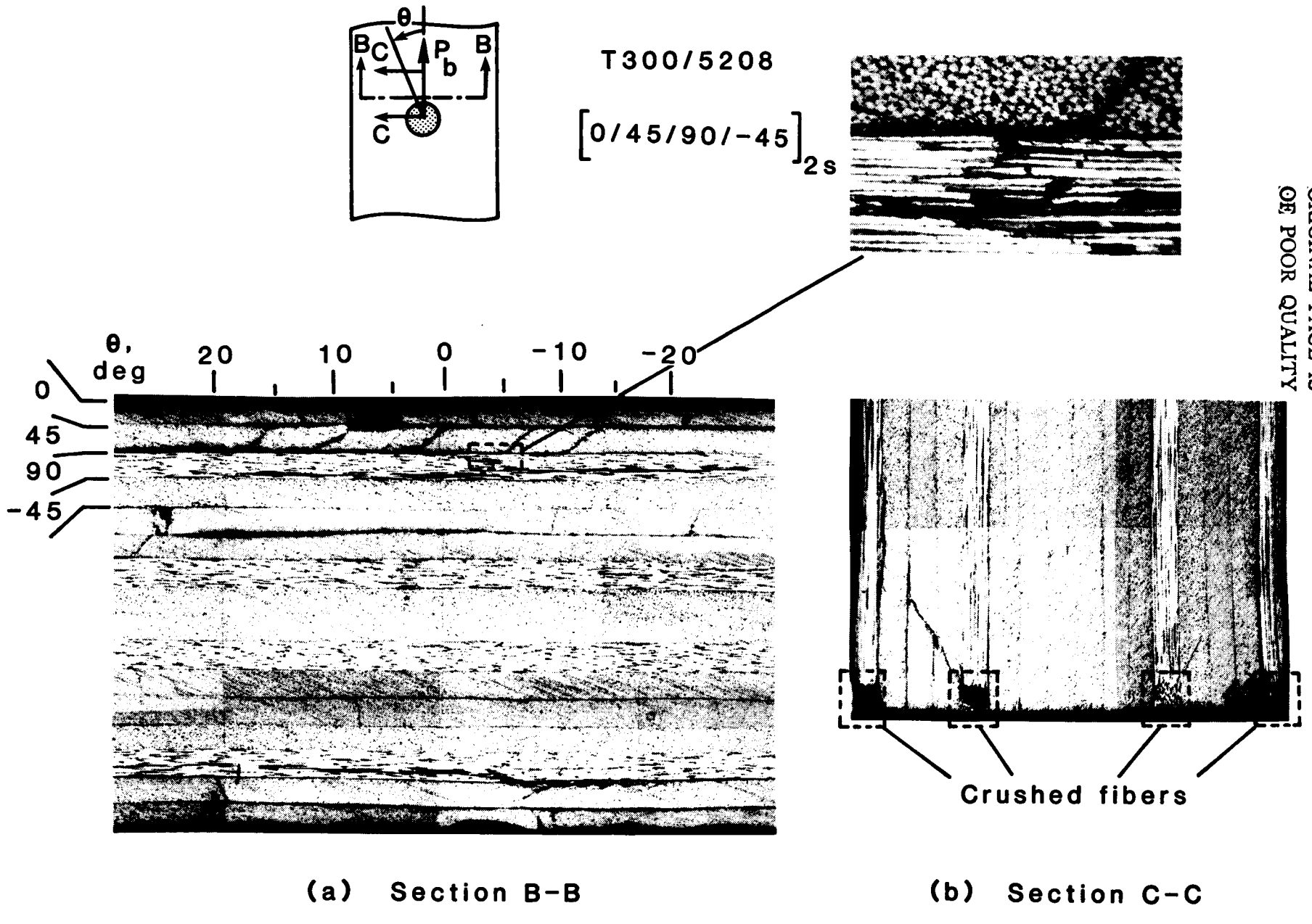

Figure 12.- Micrographs of bearing damage onset.

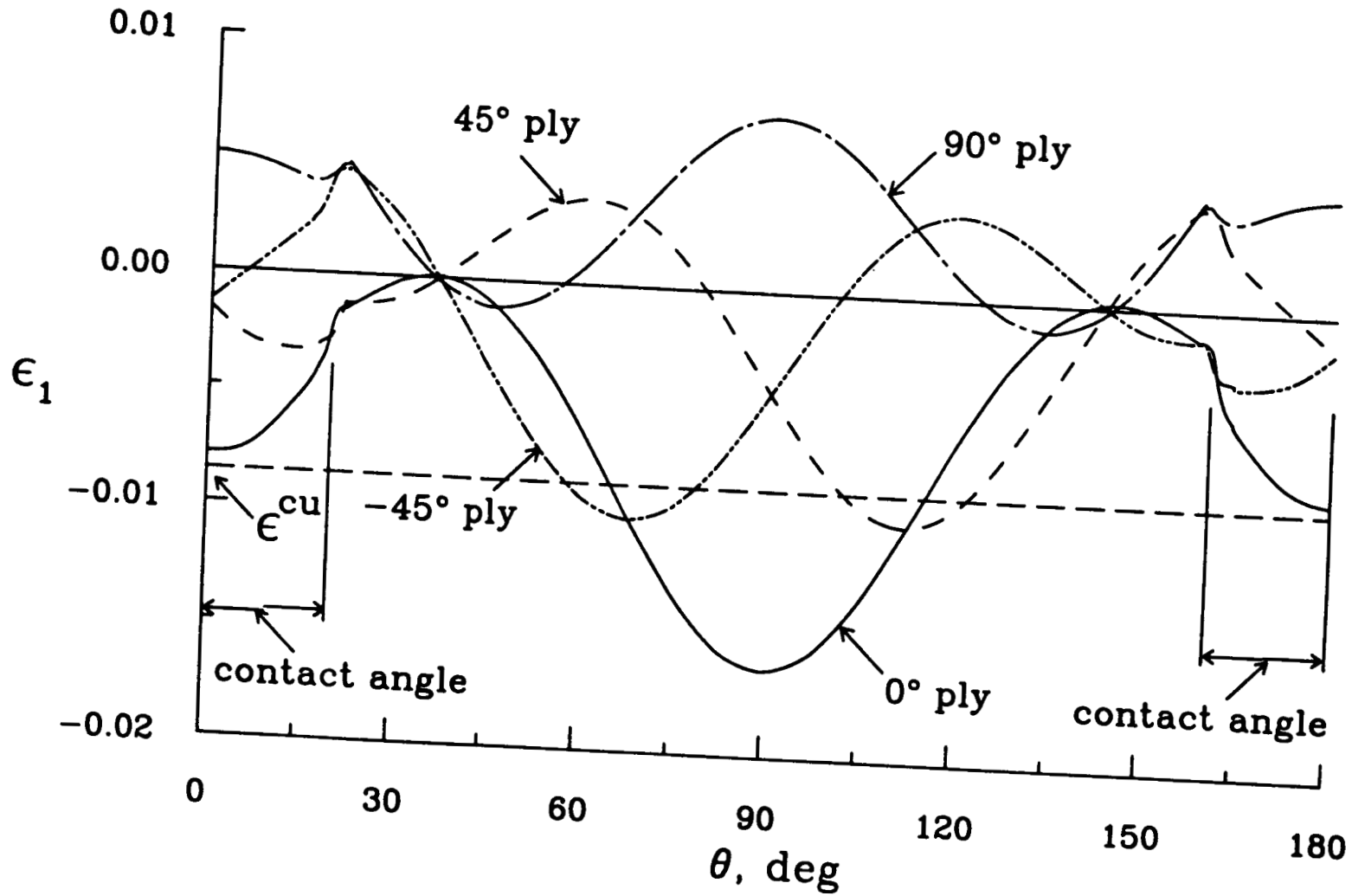

Figure 13.- Lamina ϵ_1 strains around hole boundary for NC damage onset (S_{np} = -422 MPa).

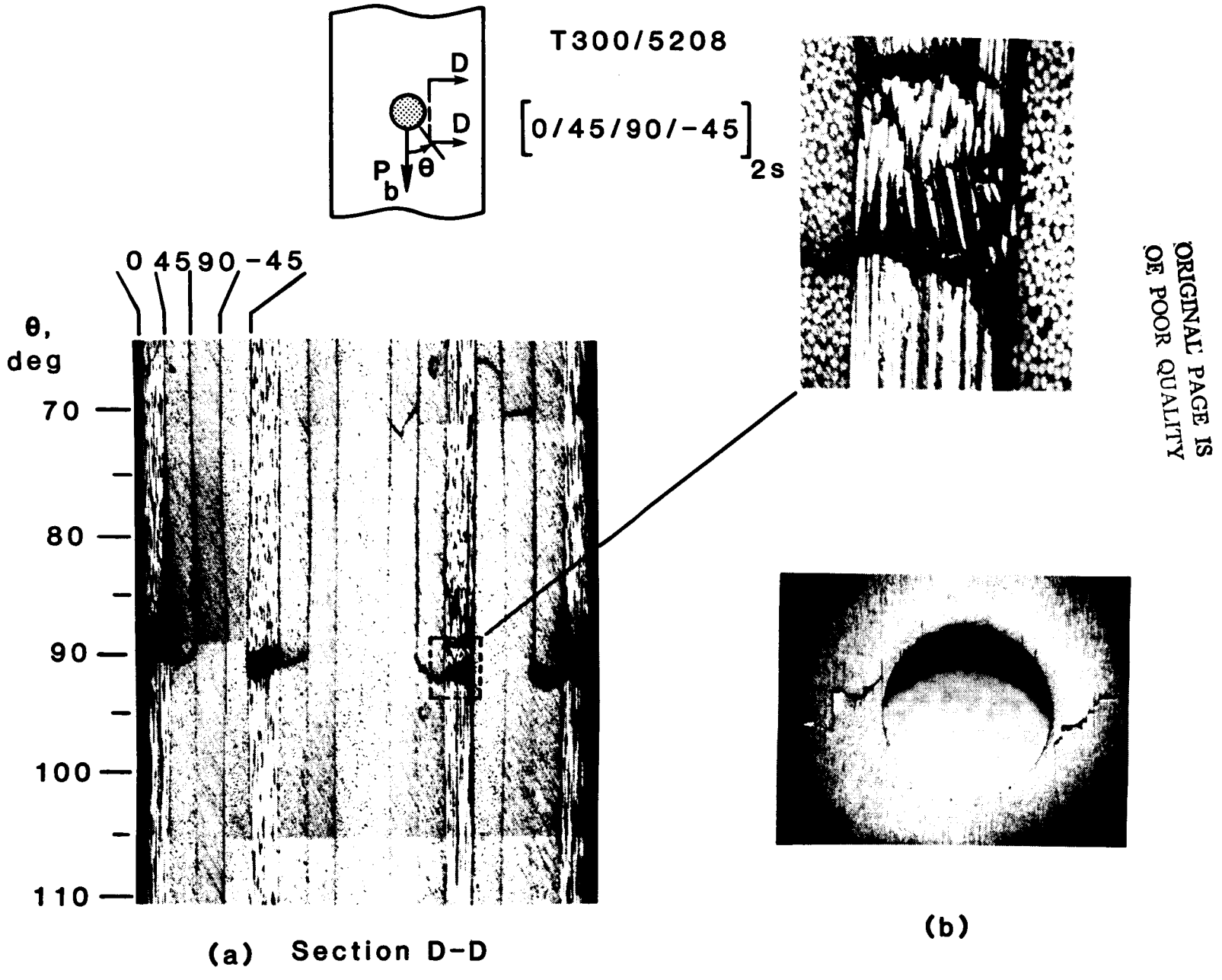

Figure 14.- Micrographs of NC damage onset.

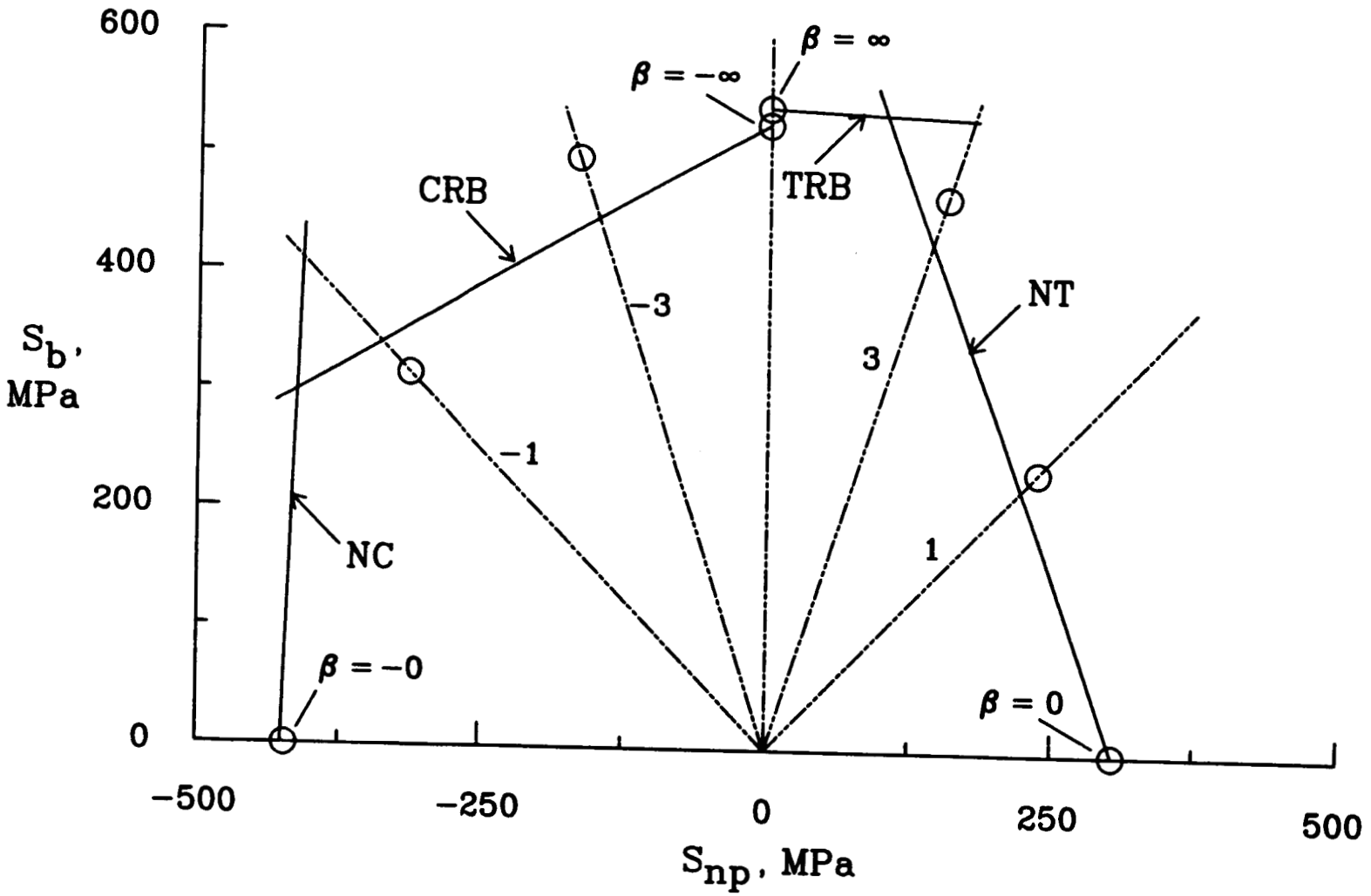

Figure 15.- Damage-onset predictions for bearing-bypass loading.

Standard Bibliographic Page

1. Report No.	2. Government Accession No.	3. Recipient's Catalog No.
NASA TM–100578		

4. Title and Subtitle	5. Report Date
PLY-LEVEL FAILURE ANALYSIS OF A GRAPHITE/EPOXY LAMINATE UNDER BEARING-BYPASS LOADING	March 1988
	6. Performing Organization Code
7. Author(s)	8. Performing Organization Report No.
R. A. Naik and J. H. Crews, Jr.	
9. Performing Organization Name and Address	10. Work Unit No.
NASA Langley Research Center Hampton, Virginia 23665-5225	505-63-01-05
	11. Contract or Grant No.
12. Sponsoring Agency Name and Address	13. Type of Report and Period Covered
National Aeronautics and Space Administration Washington, DC 20546-0001	Technical Memorandum
	14. Sponsoring Agency Code

15. Supplementary Notes

R. A. Naik, PRC Kentron, Hampton, VA
J. H. Crews, Jr., Langley Research Center, Hampton, VA

16. Abstract A combined experimental and analytical study has been conducted to investigate and predict the failure modes of a graphite/epoxy laminate subjected to combined bearing and bypass loading. Tests were conducted in a test machine that allowed the bearing-bypass load ratio to be controlled while a single-fastener coupon was loaded to failure in either tension or compression. Test coupons consisted of 16-ply, quasi-isotropic, T300/5208 graphite/epoxy laminates with a centrally-located 6.35-mm bolt having a clearance fit. Onset and ultimate failure modes and strengths were determined for each test case. The damage-onset modes were studied in detail by sectioning and micrographing the damaged specimens. A two-dimensional, finite-element analysis was conducted to determine lamina strains around the bolt hole. Damage onset consisted of matrix cracks, delamination, and fiber failures. Stiffness loss appeared to be caused by fiber failures rather than by matrix cracking and delamination. Fiber failures in the 0 deg plies in the net-section tension and net-compression modes followed the matrix cracking direction in the adjacent 45 deg plies. Fiber failures associated with bearing damage were of two different types; compressively loaded fibers in the 0 deg plies failed by crushing whereas fibers in the 90 deg plies failed in tension. An unusual offset-compression mode was observed for compressive bearing-bypass loading in which the specimen failed across its width along a line offset from the hole. The computed lamina strains in the fiber direction were used in a combined analytical and experimental approach to predict bearing-bypass diagrams for damage onset from a few simple tests.

17. Key Words (Suggested by Authors(s))
Laminate
Lamina
Bolt
Bearing
Graphite/epoxy
Strength
Damage
Stress analysis
Composites
Joint

18. Distribution Statement
Unclassified - Unlimited
Subject Category - 24

19. Security Classif.(of this report)	20. Security Classif.(of this page)	21. No. of Pages	22. Price
Unclassified	Unclassified	36	A03

For sale by the National Technical Information Service, Springfield, Virginia 22161